SECONDARY ARCING TRIGGERED BY HYPERVELOCITY IMPACTS ON SOLAR PANEL REAR SIDE CABLES WITH DEFECTS - COMPARISON WITH LASER IMPACTS

Jean-Michel Siguier[(1)], Virginie Inguimbert[(1)], Gaël Murat[(1)], Denis Payan[(2)] and Emilie Gloaguen[(2)]

[(1)]DESP, UFT-MiP, ONERA, 2 Avenue Edouard Belin, 31000 Toulouse, France, jean-michel.siguier@onera.fr

[(2)]CNES, 16 Avenue Edouard Belin, 31401 Toulouse, France, denis.payan@cnes.fr

ABSTRACT

High velocity impacts of micrometeoroids and debris are proven causes of solar arrays power loss. Many studies have been carried out in this domain with relatively large size particles, in the range of 1mm, causing obviously large damages, but with a small probability of occurrence. This paper deals with the occurrence of secondary arcing triggered on solar panel rear face cables with defects (lack of dielectric envelope) by smaller particles, in the range of 20 to 80µm (20 to 5km/s), that is with a probability of impact of several hundred of impacts by m^2 and by year both in low earth and geostationary orbits.

Plasmas produced by high velocity impacts, on metallic (aluminum) and dielectric (Kapton®) surfaces, are characterized with a Langmuir triple probe (temperature, density, floating potential, escape velocity).

Secondary arcing tests on rear side cables with cracks under high velocity impacts are achieved using a solar array simulator with realistic in flight electrical conditions (120V-1 to 3A).

Secondary arcing tests and plasma characterization are also carried out with laser impacts (0.2J YAG laser) and compared with high velocity impacts.

1. INTRODUCTION

Secondary arcing is a well-established cause of power loss on solar arrays and its occurrence is still largely studied because manufacturing and electric conditions are always evolving. If the main cause of primary arcing, which may lead to secondary arcing, is due to electrostatic discharges, another one is attributed to micrometeoroid and debris (MMD) impacts. Many studies carried out with large size projectiles (>1mm) have determined that hypervelocity impacts (HVI) create, in both sides of a solar array, defects and plasma at the same time which may trigger a secondary arc between polarized and non-protected metallic elements [1] [2] [3] [4]. Other studies performed with smaller projectiles in the range of 40 to 500µm impacting solar cell or harness coupons showed very dispersive results : inconclusive [5], without any secondary arc [6], transient sustained arc (TSA) [7] and permanent sustained arc (PSA) but with a very high (=8A) solar array simulator (SAS) value [8].

This study deals with the possibility to trigger secondary arcs on solar arrays with impacting particles in the range 20 to 80µm and to compare these hypervelocity impacts to laser impacts in order to have a more simple way to carry out experimentation than using a HVI facility.

The range 20 to 80µm is chosen because the probability is rather important (few 100 impacts/m^2/year) compared to 1mm size particles (≈ 10^{-2} impacts/m^2/year) and the plasma produced by the impact is supposed to be dense enough to trigger an arc [9].

Secondary arcs are performed on back side solar array cables with defects that is between unshielded parts of two cables polarized with a SAS.

In a first step, plasmas produced by the impact of glass projectiles on aluminum and Kapton® surfaces are characterized by a triple Langmuir probe and compared with plasmas produced by laser impacts on the same surfaces.

In a second step, secondary arcs tests are performed with HVI and laser impacts on an unshielded back side cable.

2. HVI PLASMA CHARACTERIZATION

A. Triple probe

The Langmuir triple probe we used for plasma characterization is shown on Fig. 1 and the setup on Fig. 2. Each electrode is metal covered with carbon powder, length 16mm and diameter 2.2mm. V_{21} and V_{31} values are 1.5V and 9V. R is from 100Ω to 1kΩ depending on plasma density. The oscilloscope, insulating from ground, measures the voltages induced by the three currents through the resistors. For high plasma densities (i.e. laser impacts), the three resistors and the floating oscilloscope are suppressed and replaced by transient current probes connected to a regularly grounded oscilloscope.

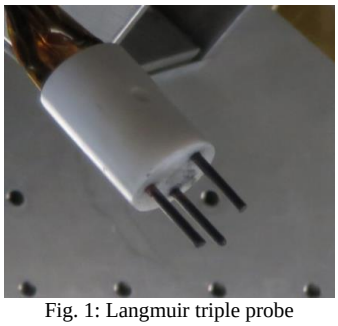

Fig. 1: Langmuir triple probe

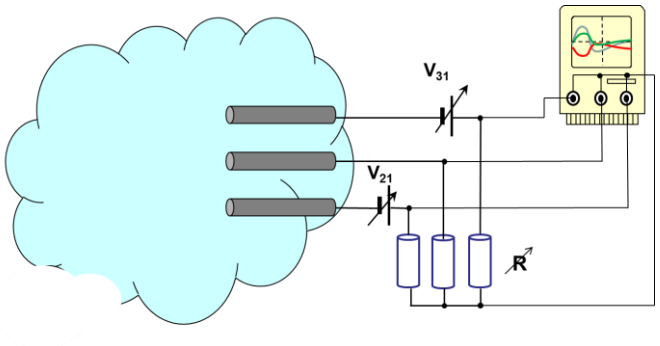

Fig. 2: triple probe setup

Triple probe theory is described on [10]. From current measurements we deduce electron temperature, T_e, plasma density, N_e, and floating potential, V_f, of the transient plasma. Calculations are detailed on [11]. The response time of the circuit is better than 1µs.

B. HVI facility

The HVI facility used for this study is a plasma-dynamic accelerator located at TUM and providing HVI of glass sphere from 20 to 80µm with corresponding velocity 2 to 20 km/s as seen on Fig. 3. The impact location is in a diameter of 5cm.

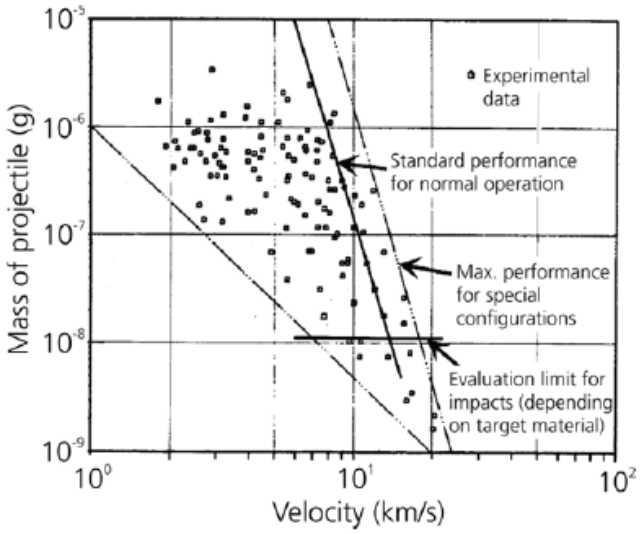

Fig. 3 mass/velocity distribution of the TUM /LRC plasma-dynamic accelerator of TUM/LRT [8]

C. HVI plasma results

The triple probe is set at about 5cm of the aluminum or Kapton film but, due to the uncertainty of the impact location (within an area of 5x5cm^2), the impact-probe distance may vary from 3 to 8cm. Several shots are performed and the velocity is measured for each shot in order to verify an average velocity of 7.1km/s which gives, from Fig. 3, an average projectile size (glass sphere) of Ø50µm.

Fig. 4 shows an example of probe currents collected during the shot. During the first 400µs the triple probe is saturated by the incident plasma coming with the glass projectile. The impact occurs at about 550µs, which gives a velocity of 8.3km/s and then, from Fig. 3, an estimated projectile size of Ø60µm ± 30µm. The plasma flow lasts few tenths of µs and reaches a maximum value which is used for plasma parameters calculation.

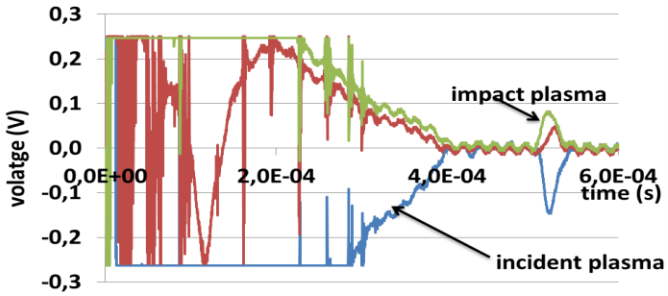

Fig. 4 : plasma currents collected by the triple probe during a HVI on 125µm Kapton film

TABLE 1 and TABLE 2 show average plasma characteristics of HVI performed on aluminum and Kapton surfaces. Standard deviation is due to both the size/velocity dispersion of the different impacts and the noisy signal.

TABLE 1: plasma characteristics of HVI on aluminum

HVI on aluminum	average	standard deviation
T_e	0,9 eV	0,2
N_e	$2{,}5.10^{14}$ m^{-3}	$1{,}1.10^{14}$ m^{-3}
V_f	2,8 V	0,7 V

TABLE 2: plasma characteristics of HVI on Kapton

HVI on Kapton	average	standard deviation
T_e	0,9 eV	0,1 eV
N_e	3.10^{14} m^{-3}	$1{,}3.10^{14}$ m^{-3}
V_f	2,7 V	0,2 V

3. LASER PLASMA CHARACTERIZATION

A. Laser facility

Plasma measurements and arcing tests with laser impact are performed in the JONAS facility (9m^3 vacuum chamber) located at DESP/ONERA-Toulouse. Laser is a YAG type providing about 0.2J focused pulse (Ø≈300µm) at 1.05nm and 20ns duration.

B. Laser impacts results

Because collected probe currents are higher than HVI for the aluminum plate and because there is more space in the facility to set several triple probes, a more significant study is carried out on laser plasma characterization. In this aim, two triple probes are set at different distances from the impact location in order to measure plasma characteristics function of distance to the impact location and the plasma escaping velocity.

Examples of plasma currents collected by the triple probes are shown on Fig. 5 and Fig. 6.

Measurements, performed at different distances from the impact location, show temperature, density and floating potential evolution versus the distance on Fig. 7, Fig. 8, Fig. 9 and Fig. 10.

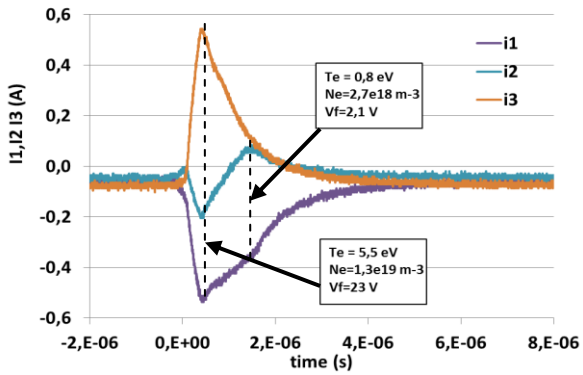

Fig. 5: collected currents at 3cm from the laser impact with plasma parameters calculations at two different times

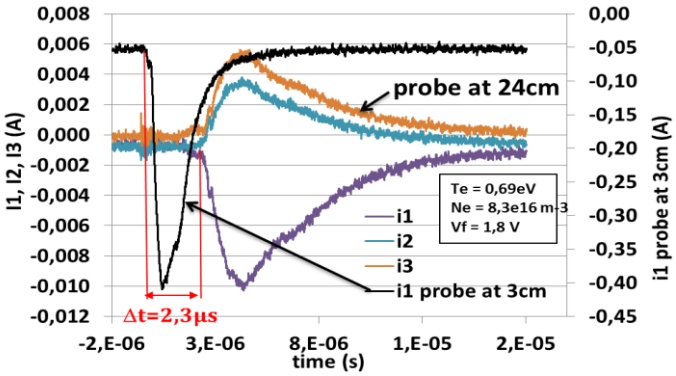

Fig. 6: collected currents at 24 cm from the laser impact and time delay evaluation with the probe at 3cm.

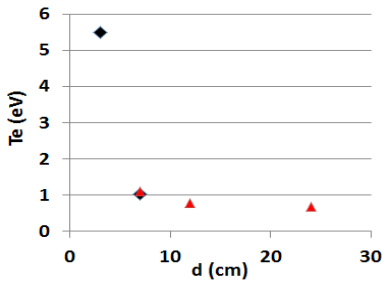

Fig. 7: electronic temperature of laser impact plasma on aluminum function of distance (probe 1 in black, probe 2 in red)

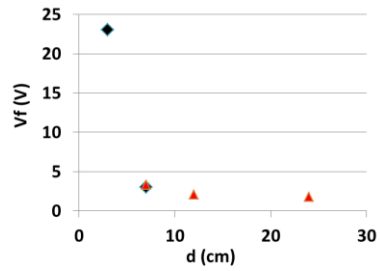

Fig. 8: floating potential of laser impact plasma on aluminum function of distance

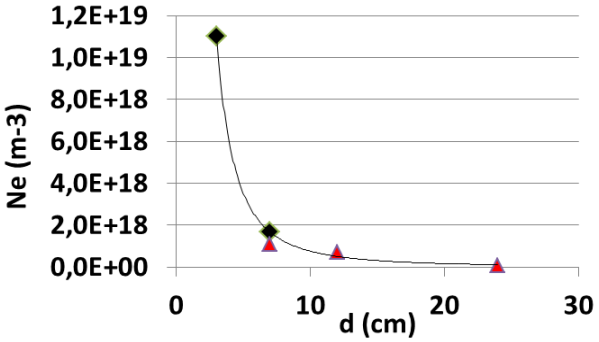

Fig. 9: density of laser impact plasma on aluminum function of distance

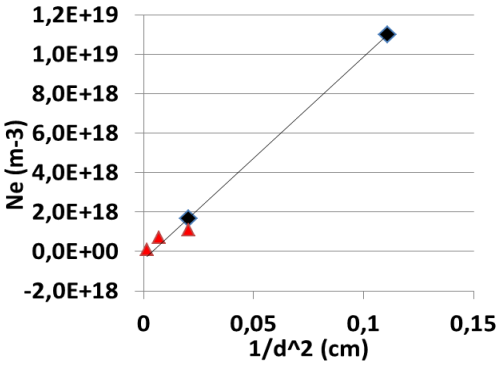

Fig. 10: density of laser impact plasma on aluminum function of $1/d^2$

4. CALCULATION OF TOTAL EMITTED CHARGES

Widening of the current pulse between the 3cm distance and the 24cm distance probe, on Fig. 6, means that the plasma produced by the impact is escaping with a distribution of velocities. Velocity of the maximum of distribution is 85±10km/s, in the same range as measured by [12]. This means that the triple probes measure an instantaneous charges density. Fig. 10 shows that the expansion is spherical so, with some geometric approximations and considering a directivity, θ, of the emitted plasma as seen on [12], we can calculate the total emitted charges by the laser impact, Q, following Fig. 11 model.

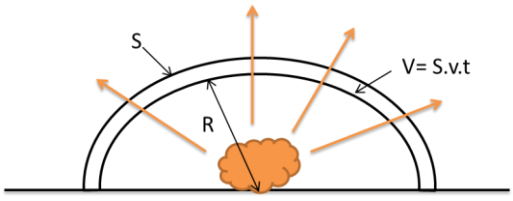

Fig. 11: plasma escape model

$$Q = \theta \int_t n(t).V.dt \approx \theta \int_t n(t).S.v.t.dt \quad (1)$$

With: Q = total number of emitted charges

V = volume crossed by the charges
n(t) = local charge density measured by the probe as a function of time
v = average escaping velocity of the charges
S = surface of the semi-sphere

That is, with discrete time steps:

$$Q \approx \theta . 2\pi . R^2 . v . \sum_i N(\Delta t_i) . \Delta t_i \qquad (2)$$

This plasma expansion model is also applied to HVI charge calculations .In this case, according to [9], plasma expansion velocity is estimated equal to the impact velocity.

5. COMPARISON HVI-LASER IMPACT PLASMA

Plasma characteristics produced by HVI and laser impacts, measured at 5cm from the impact location, are summarized in TABLE 3 for aluminum target and TABLE 4 for Kapton target.

As we can see in these tables, laser impacts (0.2J) produce much more plasma than HVI (glass, 50µm, 7km/s). Laser impact plasma depends strongly on the target material which is not the case for HVI on aluminum and Kapton. For a perforating laser impact on Kapton, we suppose that a part of the produced plasma is trapped on the back side and so less plasma is measured in the front side.

TABLE 3: comparison of HVI and laser plasma for aluminum at 5cm

aluminum :	HVI	Laser
T_e	0,9 eV	2 eV
N_e	$2.5.10^{14}$ m^{-3}	$3.10^{18} m^{-3}$
V_f	2,8 V	7 V

TABLE 4: comparison of HVI and laser plasma for Kapton at 5cm

Kapton 125 µm:	HVI	Laser (no perforating)	Laser (perforating)
T_e	0.9 eV	1.1 eV	0.6 eV
N_e	3.10^{14} m^{-3}	$1.6.10^{16} m^{-3}$	$3.10^{15} m^{-3}$
V_f	2.7 V	3.3 V	1.6 V

Plasma charges produced by HVI and laser impacts have been largely measured and modelized by empirical equations [13], [14], [15].

For HVI, the total amount of charges produced is:

$$Q(C) = 1.3.10^{-4} m^{\alpha} v^{\beta} \qquad (3)$$

with : m = projectile mass (g)
α = 0.95 (for our conditions)
v = velocity (km/s)
β = 3.5 (for our conditions)
Q is divided by 5 if the target is dielectrics. The nature of projectile is without effect on plasma production [14].

For laser impact, the total amount of charges produced is (first level of ionization):

$$Q(+) \ (mC/mm^2) = 0.58 \ln(E_1/E_0) \qquad (4)$$

with E_0= threshold depending on target nature:
E_0 = 1.0 GW/cm² for semi-conductors (C, Si)
E_0 = 1.5 GW/cm² for metals
E_0 = 4.0 GW/cm² for dielectrics
E_1 = laser pulse density

$$E_1 \left(\frac{GW}{cm^2}\right) = \frac{W}{tS} 10^{-9} \qquad (5)$$

with: W = laser pulse energy (J)
t = pulse duration (s)
s = impact surface (cm^2)

TABLE 5 compares the total number of plasma charges produced by HVI and laser impacts. Charges released by 50µm HVI are comparable to an electrostatic discharge (ESD) of 100pF (≈ GEO satellite capacitance) at 1kV and charges released by 0.2J laser impact are comparable to an electrostatic discharges (ESD) of 150µF (≈ LEO satellite capacitance) at 1kV. Range values for HVI correspond to uncertainty on projectile size and impact-probe distance. HVI presents a good matching between calculated and measured values. Difference between calculated and measured values for laser impact may be due to the uncertainty on emitted plasma directivity.

TABLE 5: comparison of total emitted charges for HVI, laser impact and electrostatic discharge (ESD)

	Incident energy	Q calculated with (3),(4) or (5)	Q measured and calculated with (2)
HVI (Ø50µm/7km/s) on aluminum	0.4mJ< Q <25mJ	25nC<Q<140nC	9nC<Q<100nC
HVI (Ø50µm/7km/s) on Kapton	0.4mJ< Q <25mJ	5nC<Q<30nC	11nC<Q<120nC
Laser (0.2 J, 20 ns, 0.03mm^2) on aluminum	200 mJ	110 µC	150 µC
Laser (0.2 J, 20 ns, 0.03mm^2) on Kapton	200 mJ	50 µC	120 µC
ESD 100pF	50 µJ	100 nC	
ESD 150nF	75 mJ	150 µC	

6. ARCING TESTS

The main point of this study is to determine if HVI of 20 to 80µm particles are able to trigger secondary arcs on cables presenting unprotected parts due to aging, manufacturing

conception or defects as it may happens on rear side solar panels.

This king of test was already performed in our lab on cables with cracks but with a secondary arc triggered by ESD in inverse potential gradient situation [16]. It showed that different types of secondary arcs occurred for specific voltage/current values of solar array simulator (SAS):

- SAS = 120V/1A, non-sustained arc (NSA) relative to primary arc duration
- SAS = 120V/2A, temporary-sustained arc (TSA) relative to primary arc duration
- SAS = 120V/3A, permanent arc (PSA)

In order to be comparative, the same setup and the same SAS values are used in this study. The differences are in the secondary arc triggering mechanism and the tested sample constitution.

A. Secondary arc test sample

The sample is constituted of two unshielded Tefzel® wires (gauge#20), separated by 1.8mm and rolled up around two nylon threaded rods in order to maximize the probability of getting an impact onto the cable (Fig. 12). The diameter of the metallic core of the Tefzel cable is about 0.7mm (see Fig. 14).

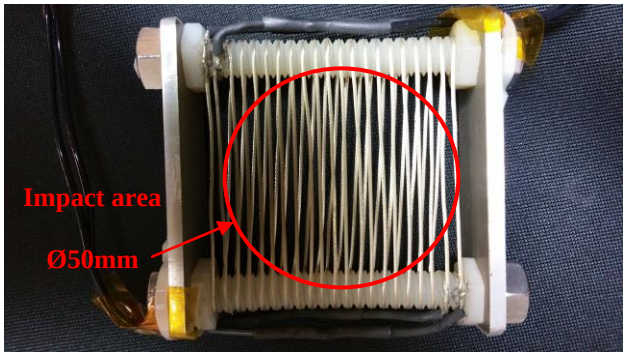

Fig. 12: secondary arcing test sample

B. Secondary arc test setup

The setup (Fig. 13) is similar to [16]. SAS voltage is set to 120V and R_c monitors the current in the cables from 1 to 3.5A (maximum bearable by our SAS).

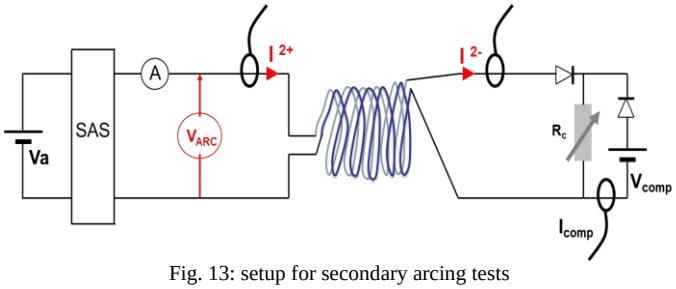

Fig. 13: setup for secondary arcing tests

C. Arcing tests with HVI

An example of impact damage on the metallic part of the Tefzel cable is showed on Fig. 14.

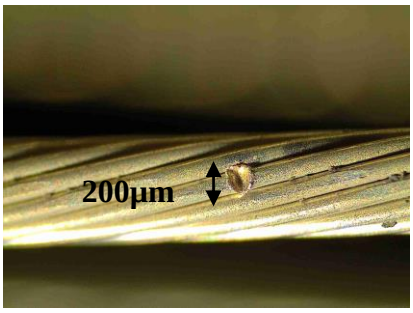

Fig. 14: hypervelocity impact damage of a glass sphere (between 20 to 80µm) on the metallic core of a Tefzel® cable.

For arcing tests, 43 shots have been performed and 15 shots impact the cables. TABLE 6 summarizes results of HVI secondary arc tests. It presents, for increasing SAS current values, duration and voltage of secondary arcs. Every HVI on cables triggers a secondary arc. As primary arc duration (= HVI plasma duration) is about 20µs (see Fig. 4), every arc is a TSA. It is remarkable that with quite low SAS current value, only 1A, we get pretty long duration secondary arc (1.4ms) but secondary arc duration does not increase with SAS current as it occurs usually. Unlike secondary arc tests triggered by ESD even high SAS current values (> 3A) do not trigger PSA, but we explain it, in Chapter 7, by the sample constitution.

TABLE 6: summary of secondary arc tests with HVI on cables

SAS values	Shot #	Impact velocity (km/s)	Arc duration (µs)	V_{arc} (V)
120 V-1.2 A	2	4.5	800	?
	5	3.1	80	40
	13	7.8	500	55
	14	1.4	120	40
	15	8.8 et 5.7 (2 impacts)	40 and 60	30 and 40
	17	**8**	**1400**	**60**
	19	4.3	400	60
120 V-2 A	20	3	280	50
	22	6	80	70
	24	**3.8**	**2000**	**50**
120 V-3 A	32	5.4	720	45
	33	5.3	500	60
	36	5.6	600	50
120 V-3.5 A	37	4.8	400	30
	41	7.4	600	30

Fig. 15 is an example of currents and voltage measured when a HVI reach the cable. The "parasitic" incident plasma coming with the high velocity particle is able to initiate an arc but not to completely establish it.

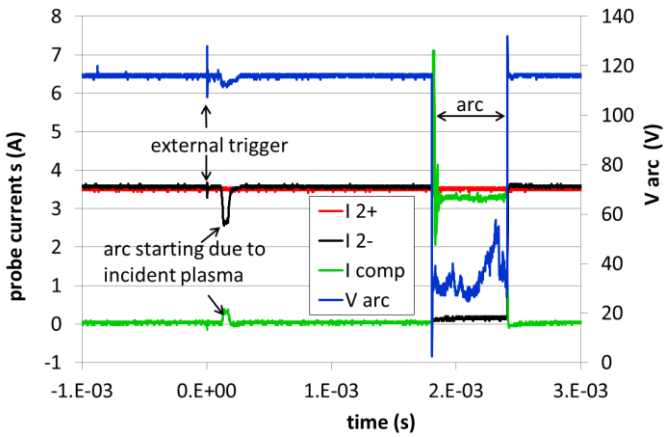

Fig. 15: example of secondary arc due to HVI (SAS: 120V/3.5A)

D. Arcing tests with laser impact

Results of secondary arcing tests triggered by laser impacts are summarized on TABLE 7.

TABLE 7: summary of secondary arc tests with laser shots on cables

SAS values	shot #	Arc duration (µs)	V_{arc} (V)
120 V-1.2 A	1	50	55
	2	100	60
	3	180	60
	4	35	40
	5	60	30
	6	60	55
	7	100	55
	8	150	55
	9	70	50
	10	30	30
120 V-2 A	1	50	40
	2	150	55
	3	160	50
	4	80	60
	5	150	60
120 V-3 A	1	740	45
	2	**1000**	**45**
	3	**1150**	**40**
	4	850	50
	5	650	40
120 V-3.5 A	1	650	50
	2	650	50
	3	**2900**	**25**
	4	**4700**	**25**
	5	**1800**	**25**
	6	**3200**	**25**
	7	**1900**	**25**
	8	400	25

As for HVI arcing tests, each impact triggers a secondary arc. Secondary arc duration increases with SAS current values. Primary arc duration is here less than 4µs, as seen by the probe at 3cm on Fig. 5, so every secondary arc is considered as a TSA, as for HVI impact.

7. Discussion

The main result of this study is that even a "small" high velocity particle triggers a secondary arc between two unshielded cables. Unfortunately, because of the strong directivity of emitted plasmas, both for HVI and laser impacts, it is not possible from our results to interpolate what is the plasma density at 1.8mm from the impact location which triggers secondary arc. Despite the plasma density difference between the two types of impacts, secondary arcing results are quite similar.

The situation of two adjacent unshielded polarized cables is not so common in solar panel rear sides but due to aging and other possible sources of defects, it is realistic. Thus, considering the large probability of "small" MMD impacts, the risk of secondary arc occurrence has to be considered seriously.

The fact that no PSA were triggered with relatively high SAS current values can be explained by the sample constitution. In this study the cables are completely unshielded in order to increase the probability of impact and thus the secondary arcing occurrence possibility. In ESD triggered secondary arc tests, leading to PSA [16] [17], only a small length of the cables (<10mm) is unshielded, the rest of the cable is still covered with a dielectric sheath. The core of the cable is not able to provide, by cathodic spot emission, enough metallic vapors to maintain an arc pressure. A gas inflow as for plasma torch [18] or an expendable "wall" material [19] as the Tefzel sheath, are necessary to feed and thus maintain an arc. Here, once all the oxides and contaminants of the metal core surface are evaporated, the arc stops.

Concerning the simulation of HVI by laser impacts for arcing tests and considering only plasma production - mechanical effects are obviously strongly different - we can say that, for this range of particles (Ø20 to 80µm):

- for any kind of target materials, plasma densities are higher with a 0.2J laser beam but it is possible to reduce the plasma produced by the laser with an attenuator or by defocusing the beam,

- plasma temperatures are quite similar,

- although we did not investigate this point, it is known that directivity of the emitted plasma is sharper with laser beam than with HVI due to the fact that laser beam gives a higher kinetic energy to the plasma [12] [20].

- plasma escape velocities are higher with a laser beam than with HVI [12] [20].

Considering all these remarks, and the very similar results we got in secondary arc testing, it is possible to perform secondary arcing tests with laser impacts simulating HVI, providing that HVI defect are already simulated and that the coupon geometry does not present plasma directivity dependence.

8. SUMMARY

The first part of this study analyses and compares plasma produced by hypervelocity impacts (Ø20 to 80µm projectiles) and laser impacts (0.2J pulses). Plasma characteristics (temperature, density and floating potential) are measured with a triple probe. Total number of charges produced by both impact types are deduced from triple probe measurements and compared with theory.

The second part presents results of secondary arcing tests, triggered by hypervelocity and laser impacts, performed on unshielded solar panel cables. Temporary sustained arcs are detected with both high velocity and laser impacts, for realistic SAS values starting from 100V/1A. Permanent arcs would have certainly occur, as for ESD induced secondary arc tests, if the sample were not modified for practical reasons.

The comparison between high velocity and laser impacts for secondary arc testing is also discussed.

ACKNOWLEDGMENT

Thanks to Dr. Martin Rott (LRT, Technic University of Munich, Germany) for making us available the plasma-dynamic particle accelerator facility.

REFERENCES

[1] T. Harano, Y. Machida, S. Fukushige, T. Koura, S. Hosoda, M. Cho, et Y. Akahoshi, « Preliminary study on sustained arc due to plasma excited by hypervelocity impact of space debris on the solar array coupon », *Int. J. Impact Eng.*, vol. 33, n° 1‑12, p. 326‑334, déc. 2006.

[2] R. Putzar, F. Schaefer, et M. Lambert, « Vulnerability of spacecraft harnesses to hypervelocity impacts », *Int. J. Impact Eng.*, vol. 35, n° 12, p. 1728‑1734, déc. 2008.

[3] Y. Akahoshi, T. Nakamura, S. Fukushige, N. Furusawa, S. Kusunoki, Y. Machida, T. Koura, K. Watanabe, S. Hosoda, T. Fujita, et M. Cho, « Influence of space debris impact on solar array under power generation », *Int. J. Impact Eng.*, vol. 35, n° 12, p. 1678‑1682, déc. 2008.

[4] S. Fukushige, Y. Akahoshi, K. Watanabe, T. Nagasaki, K. Sugawara, T. Koura, et M. Cho, « Solar-Array Arcing Due to Plasma Created by Space-Debris Impact », *IEEE Trans. Plasma Sci.*, vol. 36, n° 5, p. 2434‑2439, oct. 2008.

[5] Brandhorst, « Hypervelocity impact studies of high voltage solar array segments », in *53rd International Astronautical Congress*, Houston, Texas, United States., 2002.

[6] S. Kawakita, G. Segami, K. Nitta, H. Kusawake, M. Takahashi, H. Matsumoto, et S. Hasegawa, « Discharge of Spacecraft Solar Panels by Hypervelocity Impact », *Trans. Jpn. Soc. Aeronaut. Space Sci. Space Technol. Jpn.*, vol. 7, n° ists26, p. Tr_2_53‑Tr_2_56, 2009.

[7] M. J. Neish, M. Takahashi, H. Maejima, H. Kusawake, S. Kawakita, et T. Goka, « Tests to Assess the Vulnerability of ADEOS-2 and ETS-8 to Debris and Micrometeoroid Impacts », présenté à 4th European Conference on Space Debris, 2005, vol. 587, p. 705.

[8] M. Schimmerohn, « Susceptibility of solar arrays to micrometeorite impact ». ESA contract 22462/09/NL/GLC, 2012.

[9] H. B. Garrett et S. Close, « Impact-Induced ESD and EMI/EMP Effects on Spacecraft - A Review », *IEEE Trans. Plasma Sci.*, vol. 41, n° 12, p. 3545‑3557, déc. 2013.

[10] S.-L. Chen et T. Sekiguchi, « Instantaneous Direct-Display System of Plasma Parameters by Means of Triple Probe », *J. Appl. Phys.*, vol. 36, n° 8, p. 2363‑2375, août 1965.

[11] V. Inguimbert, J. M. Siguier, G. Murat, S. Reyjal, J. C. Matéo-Vélez, P. Sarrailh, N. Balcon, et D. Payan, « Measurements of physical parameters characterizing ESDs on solar cell and correlation between spectral signature and discharge position », *IEEE Trans. Plasma Sci.*, vol. 43, n° 9, p. 2985‑2992, sept. 2015.

[12] O. Albert, S. Roger, Y. Glinec, J. C. Loulergue, J. Etchepare, C. Boulmer-Leborgne, J. Perrière, et E. Millon, « Time-resolved spectroscopy measurements of a titanium plasma induced by nanosecond and femtosecond lasers », *Appl. Phys. A*, vol. 76, n° 3, p. 319‑323, mars 2003.

[13] J. Kissel et F. R. Krueger, « Ion formation by impact of fast dust particles and comparison with related techniques », *Appl. Phys. A*, vol. 42, n° 1, p. 69‑85, janv. 1987.

[14] F. R. Krueger, « Hypervelocity Impact Physics - Plasma Discharge Phenomena on Solar Generators », in *The Behavior of Systems in the Space Environment*, R. N. DeWitt, D. Duston, et A. K. Hyder, Éd. Springer Netherlands, 1993, p. 273‑290.

[15] P. R. Ratcliff, M. J. Burchell, M. J. Cole, T. W. Murphy, et F. Alladfadi, « Experimental measurements of hypervelocity impact plasma yield and energetics », *Int. J. Impact Eng.*, vol. 20, n° 6‑10, p. 663‑674, 1997.

[16] J.-M. Siguier, V. Inguimbert, G. Murat, D. Payan, et N. Balcon, « Study of secondary arcing occurrence on solar panel backside wires with cracks », *IEEE Trans. Plasma Sci.*, vol. 43, n° 9, p. 2980‑2984, sept. 2015.

[17] D. Qu, K. Tomoki, S. Aso, et Okomura T., « Laboratory test of arcing on satellite power cables », présenté à 9th SCTC, Tsukuba Japan, 2005.

[18] J. P. Trelles, C. Chazelas, A. Vardelle, et J. V. R. Heberlein, « Arc Plasma Torch Modeling », *J. Therm. Spray Technol.*, vol. 18, n° 5‑6, p. 728‑752, juin 2009.

[19] C. B. Ruchti et L. Niemeyer, « Ablation Controlled Arcs », *IEEE Trans. Plasma Sci.*, vol. 14, n° 4, p. 423‑434, août 1986.

[20] M. Rival et J. C. Mandeville, « Modeling of Ejecta Produced upon Hypervelocity Impacts », *Space Debris*, vol. 1, n° 1, p. 45‑57, mars 1999.